

ACCEPTED MANUSCRIPT

## Real-time position and pose prediction for a self-propelled undulatory swimmer in 3D space with artificial lateral line system

To cite this article: Ruosi Liu *et al* 2024 *Bioinspir. Biomim.*



During the embargo period (the 12 month period from the publication of the Version of Record of this article), the Accepted Manuscript is fully protected by copyright and cannot be reused or reposted elsewhere.

As the Version of Record of this article is going to be / has been published on a subscription basis, this Accepted Manuscript will be available for reuse under a CC BY-NC-ND 3.0 licence after the 12 month embargo period.

After the embargo period, everyone is permitted to use copy and redistribute this article for non-commercial purposes only, provided that they adhere to all the terms of the licence <https://creativecommons.org/licenses/by-nc-nd/3.0>

Although reasonable endeavours have been taken to obtain all necessary permissions from third parties to include their copyrighted content within this article, their full citation and copyright line may not be present in this Accepted Manuscript version. Before using any content from this article, please refer to the Version of Record on IOPscience once published for full citation and copyright details, as permissions may be required. All third party content is fully copyright protected, unless specifically stated otherwise in the figure caption in the Version of Record.

View the [article online](#) for updates and enhancements.

# Real-time position and pose prediction for a self-propelled undulatory swimmer in 3D space with artificial lateral line system

Ruosi Liu<sup>1</sup>, Yang Ding<sup>2,3</sup> and Guangming Xie<sup>1,4</sup>

State Key Laboratory for Turbulence and Complex Systems, College of Engineering, Peking University, Beijing, People's Republic of China<sup>1</sup>

Beijing Computational Science Research Center, Haidian District, Beijing, People's Republic of China<sup>2</sup>

Beijing Normal University, Haidian District, Beijing, People's Republic of China<sup>3</sup>

Institute of Ocean Research, Peking University, Beijing, People's Republic of China<sup>4</sup>

E-mail: xiegm@pku.edu.cn and dingyang@csrc.ac.cn

## Abstract.

This study aims to investigate the feasibility of using an artificial lateral line system for predicting the real-time position and pose of an undulating swimmer with Carangiform swimming patterns. We established a 3D Computational Fluid Dynamics simulation to replicate the swimming dynamics of a freely swimming mackerel under various motion parameters, calculating the corresponding pressure fields. Using the simulated lateral line data, we trained an artificial neural network to predict the centroid coordinates and orientation of the swimmer. A comprehensive analysis was further conducted to explore the impact of sensor quantity, distribution, noise amplitude and sampling intervals of the artificial lateral line array on predicting performance. Additionally, to quantitatively assess the reliability of the localization network, we trained another neural network to evaluate error magnitudes for different input signals. These findings provide valuable insights for guiding future research on mutual sensing and schooling in underwater robotic fish.

## 1. Introduction

In fluid environments, the presence of swimmers, obstacles, and boundaries induces local flow alterations, enabling hydrodynamic sensing. In comparison to sonar-based or vision-based detection and localization methods, hydrodynamic sensing holds the advantage of not relying on an active emitter. Indeed, hydrodynamic sensing is a prevalent mechanism observed in numerous aquatic organisms [8, 9, 11, 28]. The lateral line system in fish, composed of superficial neuromasts (SNs) that identify velocity and canal neuromasts (CNs) that identify pressure gradients [4, 5], serves as an excellent example of the sensory system. Using the lateral line system, fish can respond to various flowing stimuli, such as cave fish navigating without relying on visual cues

1  
2  
3 *Author guidelines for IOP Publishing journals in L<sup>A</sup>T<sub>E</sub>X 2<sub>ε</sub>* 2

4 [18, 19]. Given the limitations of visual sensing in various scenarios, hydrodynamic  
5 sensing emerges as a valuable component of an integrated sensing system for robots,  
6 particularly in unstructured environments.  
7  
8  
9

10 Substantial efforts have been invested in the development of artificial lateral line  
11 (ALL) systems, often leveraging pressure sensors and/or shear sensors[13, 33, 34]. The  
12 ALL can serve as either a stationary sensor array or, similar to its biological counterpart,  
13 be attached to a moving vessel, depending on the specific detection task. The sensor  
14 array typically encompasses a range of 9 to 20 sensors, and its application spans various  
15 tasks, either experimentally or in simulation, relying on pressure or shear information.  
16 Hydrodynamic sensing applications have demonstrated success in tasks such as flow  
17 and object classification[10, 26, 29], flow velocity detection[14], carrier motion state  
18 estimation[14, 35], tracking of moving spheres[11, 30], and the precise localization of  
19 vibrating dipole sources [31, 33]. Dipole sources can accurately replicate the oscillatory  
20 movement of fish tails, serving as a crucial method for the research of fish locomotion.  
21 Initially, Yen treated the robotic fish tail as a dipole source and proposed a control  
22 method to enable it to follow another dipole source with desired phase difference[32]. Liu  
23 integrated ALLs onto a 3D-printed shell and achieve tracking of a moving dipole source,  
24 albeit limited to scenarios where the oscillating source frequency, amplitude, oscillation  
25 direction, and size are known[16]. Abdulsadda investigated an analytical model-based  
26 estimation approach, enabling the tracking of a dipole source's position even when its  
27 velocity and amplitude are unknown[1]. Qiu integrated ALLs onto robotic fish, allowing  
28 it to locate dipole sources while swimming freely[21]. While significant progress has  
29 been made in research based on dipole sources, it is essential to acknowledge that the  
30 dipole source merely serves as a simplified model of fish tail oscillation. There still  
31 exists considerable disparity between this model and the actual swimming behavior of  
32 fish. Therefore, sustained efforts are required to investigate the complex fluid-structure  
33 interaction effects between fish and water flow.  
34  
35  
36  
37  
38  
39  
40  
41  
42

43 Initial studies have employed an analytical approach, delving into flow field analysis  
44 to discern crucial flow characteristics such as zero and maximal points[11]. However,  
45 such approach is typically applicable only to inviscid scenarios and simple objects, such  
46 as spheres or dipole sources. In recent years, more advanced pattern recognition and  
47 matching techniques, such as beamforming technique[7] and template matching[6, 20],  
48 have been successfully employed. The recent advancements in machine learning,  
49 particularly in deep neural networks (DNN), have facilitated the intricate capture of  
50 complex patterns and the acquisition of substantial non-linear mappings from extensive,  
51 high-dimensional datasets. DNN approaches have been effectively implemented in  
52 various applications, including the classification of wake types (2S, 2P, etc.)[3],  
53 localization of a passing sphere in 2D [30], and the shape classification of objects passing  
54 through a 2D space [29]. However, artificial systems' sensing capabilities still fall short of  
55 those found in animals. In existing studies, certain degrees of freedom of the swimmer  
56  
57  
58  
59  
60

Author guidelines for IOP Publishing journals in  $\LaTeX 2\epsilon$

3

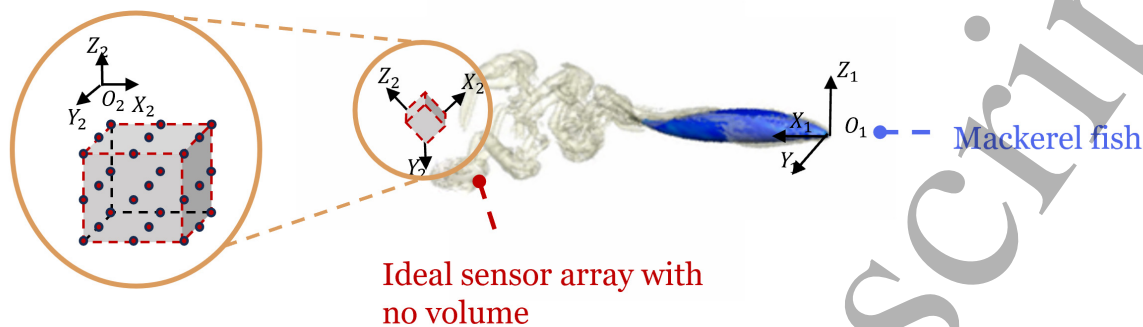


**Figure 1. The perception of a freely swimming mackerel by the ALL array.** We configured an idealized ALL array in a cubic arrangement, disregarding its volume and influence on the flow field. A mackerel, swimming freely, passes alongside the array in an arbitrary direction. Through CFD simulations, hydrodynamic information regarding the flow field was extracted during the fish's movement, simulating the signal input to the ALL. Leveraging flow field information, the swimmer's position and pose were systematically tracked in a continuous manner.

are often constrained, and there is no significant variation in the spatial relationship between the target and the swimmer [22]. Persistent efforts are needed to achieve more diverse tasks with enhanced performance, ultimately surpassing the capabilities of their biological counterparts. In this article, we demonstrate the feasibility of continuously predicting the position and pose of a freely swimming mackerel over a period of time and explore critical design parameters. A Long Short Term Memory (LSTM) neural network is trained based on local pressure information. We compare the predicting performance with different sensor quantity, Signal-to-Noise ratio, sampling time and region size. An additional network is trained to evaluate the confidence of the predictions.

## 2. Method

### 2.1. Input data

Our input data is derived from a three-dimensional CFD simulation of a Carangiform swimmer in free space (see Fig. 1). The shape and kinematics of the swimmer model are based on scans of real fish and biological observations. The swimmer's deformation follows a traveling wave pattern, expressed as  $A(s) = a_0 + a_1s + a_2s^2$ . The parameters for  $A(s)$  are meticulously adjusted to replicate the amplitude envelope observed in real fish [12, 25], with specific values of  $a_0 = 1$ ,  $a_1 = -3.2$ ,  $a_2 = 5.6$ , and  $k = 2\pi/1.0$ . The swimmer exhibits free locomotion in water, with its motion governed by the Newton-Euler equations. The fluid dynamics problem is solved using the finite difference method, incorporating the immersed boundary method to couple the swimmer with the fluid. Dimensionless units are employed, with the swimmer's body length (BL) serving as

**Table 1.** The kinematics parameters of the simulation cases

| Case No.  | 1           | 2         | 3         | 4     | 5     | 6         |
|-----------|-------------|-----------|-----------|-------|-------|-----------|
| $A$       | $A_c = 0.2$ | $1.05A_c$ | $0.95A_c$ | $A_c$ | $A_c$ | $1.05A_c$ |
| $\lambda$ | 1.0         | 1.0       | 1.0       | 1.05  | 0.95  | 0.95      |

the length unit and the undulation period standardizing the time unit. The viscosity, denoted by  $\nu$ , is set to  $1/15000$ , resulting in a corresponding Reynolds number around 4000. The swimming speed is about 0.3 BL per cycle. This simulation has been employed and validated in prior studies [17, 23].

To accumulate a substantial dataset suitable for training, we utilized a coordinate transformation approach to obtain pressure information perceived by sensors at various positions with respect to swimmers in different orientations. The ALL system can function either as a stationary sensor array or, akin to its biological counterpart, be attached to moving objects depending on the specific detection tasks. Here, following the former method, we arrange the sensors in a cubic grid across all or selected grid points, forming a sensor array as illustrated in Figure 1. The sensor array is placed within the wake of the swimming fish, acquiring pressure information from the wake to predict the position and orientation of the swimming fish. For the flow field generated through simulation, we began by randomly placing a point near the swimmer to serve as the center of the array and selecting a random direction as the orientation. Here, the volume of the sensors and their impact on the flow field were disregarded. After determining the number and arrangement of the sensor array, we recorded the pressure signals at each sensor's location when the swimmer passed by as the data collected by the ALL. The relative position of the swimmer to the sensors' center was then transformed from the swimmer's coordinate system to the local coordinate system of the sensor array. As a result, 8000 sets of trajectories with different random orientations of the swimmer were generated. For each trajectory, we segmented it into time series with a time interval of 0.025 and a total of 30 time points, corresponding to 0.75 periods of undulation. To enhance the robustness and generality of predictions, we slightly varied the kinematics parameters, with specific details provided in Table 1.

## 2.2. Prediction neural network

For the analysis of time series, we adopted the widely-used LSTM neural network. Conventional Recurrent Neural Networks (RNNs) serve as an extension to feed-forward neural networks for dynamic classification tasks, limited in their ability to look back in time due to issues like vanishing or exploding signals. LSTM was introduced as a strategic resolution to these impediments, with its fundamental concept centered around the preservation of the cell state [24], as shown in Fig. 3. As time progresses, the cell state is updated in a manner that retains important input information while forgetting unimportant and outdated information. The specific structural parameters

Author guidelines for IOP Publishing journals in  $\LaTeX 2\epsilon$

5

**Table 2.** The structural parameters of the LSTM network

| Parameter | Number of layers | Number of nodes | Dropout rate | Batch size | Learning rate | Optimizer | Loss function |
|-----------|------------------|-----------------|--------------|------------|---------------|-----------|---------------|
| Value     | 2                | 200             | 0.1          | 64         | 0.001, 0.0001 | Adam      | MSE           |

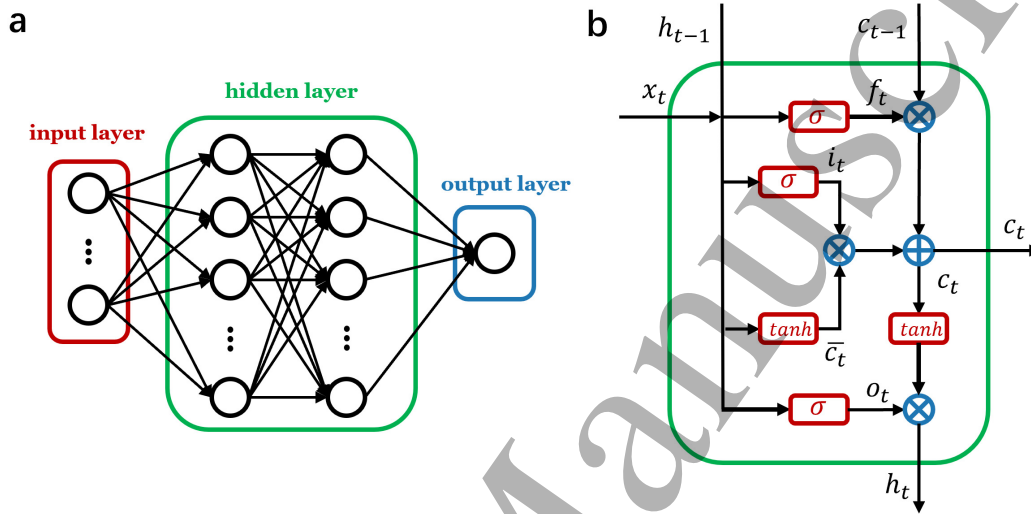


**Figure 2.** (a) **Structure of RNN.** RNNs range from partly to fully connected, typically incorporating three components: the input layer, the hidden layer, and the output layer. (b) **Structure of LSTM.** LSTM is a distinctive type of RNN, characterized by its use of a cell state to preserve essential information while discarding less relevant portions.

of the network is shown in Table 2. In this context, the network takes simulated pressure information as input and outputs a six-dimensional vector consisting of the fish's current centroid coordinates and velocity direction at the present moment. We employed a dropout rate of 0.1 during training to prevent over-fitting. After 100 epochs, the residual values stabilized.

### 2.3. Error estimation network

For any input, the neural network generates a prediction, necessitating a systematic approach to gauge its confidence. At least, a method is needed to determine if information can be gleaned from the input signal and to discern the reliability of predictions. Here, we propose a similar approach: employing another LSTM neural network with identical inputs, we train it to predict errors in position and pose predictions, offering a quantitative measure of confidence. The natural metric for prediction errors is the distance  $\Delta$  between the actual and predicted positions of the swimmer. However, in instances of complete unreliable predictions, the associated error becomes unbounded. An additional consideration is the effective range of the lateral line, limited to a few body lengths, where errors surpassing this threshold

1  
2  
3 *Author guidelines for IOP Publishing journals in L<sup>A</sup>T<sub>E</sub>X 2<sub>ε</sub>* 6

4 indicate unreliable predictions. Consequently, we employ the  $\Delta_c = \tanh(2\Delta)$  function  
5 to compress errors at the large end, directing our focus towards prediction confidence.  
6 This methodology uniformly integrates cases of complete unreliability while concurrently  
7 incorporating instances where predictions exhibit a certain level of reliability. In training  
8 the confidence network, we maintain the prediction network constant, utilizing actual  
9 errors as the training dataset. Notably, 10% of the training data comprises null data,  
10 exemplified by white noise with an amplitude equivalent to 5% of the input.  
11  
12  
13  
14

### 15 **3. Results**

#### 16 *3.1. Predictions on position and pose*

17  
18 The distribution of pressure within the vortex is shown in Fig.3a. As depicted, the  
19 pressure within the vortex exhibits a unique spatial structure, displaying identifiable  
20 features. Over time, this pressure structure propagates in the opposite direction of the  
21 fish's movement, accompanied by a significant decrease in amplitude. These features  
22 suggest the presence of discernible patterns within the pressure field, closely linked to  
23 the position and orientation of the preceding fish.  
24  
25  
26  
27  
28

29 We utilize the centroid coordinates of the fish and the direction vector to represent its  
30 position and orientation (Fig. 3b), respectively. The coordinates of the fish body's  
31 centroid in the sensor coordinate system are represented by  $\vec{x}$ ,  $\vec{y}$ , and  $\vec{z}$ . The  
32 direction vector of the fish body's velocity is denoted by  $\vec{V}$ , with  $V_x\vec{e}_x$ ,  $V_y\vec{e}_y$ , and  
33  $V_z\vec{e}_z$  as its components along three coordinate axes. Fig. 3c depicts the progressive  
34 reduction of training error with increasing epochs, indicating robust convergence in  
35 the model. After 50 epochs, the rate of change slows down, and by 300 epochs, it  
36 reaches a plateau. The loss value of the plateau is about 0.001, corresponding to an  
37 average error of 0.03 BL. Fig. 3d illustrates the predictive capability of the positioning  
38 neural network PredNet over a certain period. As a reference, the solid line represents  
39 the actual values. The outcomes reveal that, throughout the entire swimming duration,  
40 PredNet consistently and accurately traces the fish's location and orientation, indicating  
41 its ability to effectively capture position and pose information within the pressure field.  
42  
43  
44  
45  
46  
47

#### 48 *3.2. Impact of sensing region size*

49 The arrangement of the sensor array significantly impacts the effectiveness of  
50 information gathering[15], with one crucial factor being the distance between adjacent  
51 sensors, influencing the dimensions of the entire ALL system. Clearly, a larger sensor  
52 distance results in more distinctive information, enhancing the richness of acquired data  
53 with the same quantity of sensors. However, this inevitably leads to an enlarged ALL  
54 array, posing greater manufacturing challenges and costs, along with potential risks such  
55 as a more pronounced impact on the flow field structure and increased detectability by  
56 other entities. Here, we quantitatively compare the positioning performance of the ALL  
57  
58  
59  
60

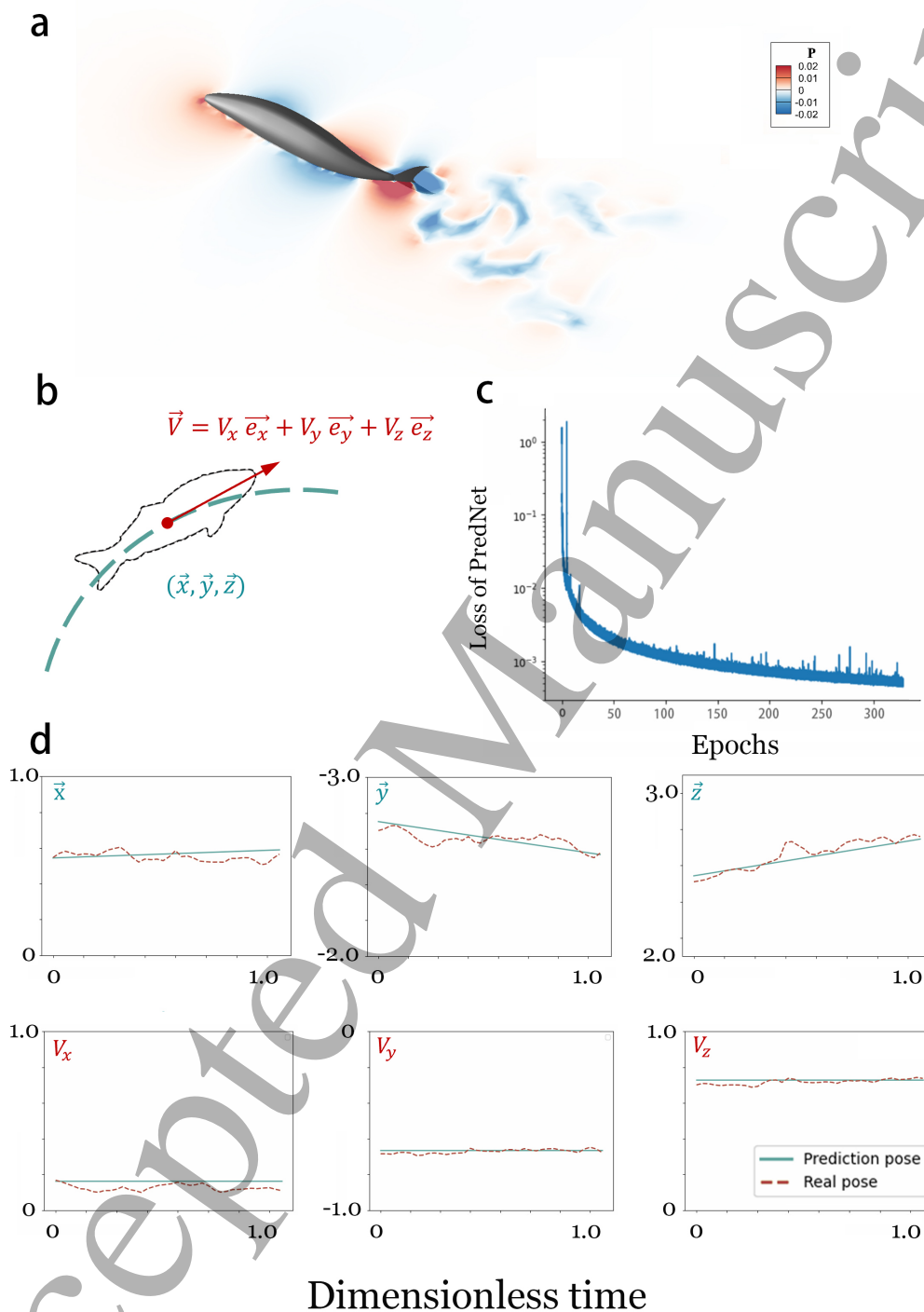


**Figure 3. Prediction of Fish Body Position and Pose** (a) The spatial distribution of pressure in the surroundings of the fish's body. (b) Diagram illustrating the representation of fish position and orientation. (c) Training loss as a function of epochs. (d) Example predictions of PredNet for the fish body coordinates and the direction vector over a certain period. The actual values are also provided as a reference.

1  
2  
3 *Author guidelines for IOP Publishing journals in L<sup>A</sup>T<sub>E</sub>X 2<sub>ε</sub>* 8

4 under different distances. As shown in Fig. 5b, the error gradually decreases with  
5 increasing distance, aligning with our expectations. This decline begins to plateau after  
6 reaching 0.02BL and almost halts after reaching 0.1BL.  
7  
8  
9

### 10 *3.3. Impact of sensor quantity*

11 Initially, an analysis was conducted to assess the impact of the number of sensors on  
12 predictive performance. In most cases, maintaining consistency in the arrangement  
13 while studying quantity relationships poses a significant challenge. In this study, we first  
14 examined the results when the sensor array maintained a consistent cubic configuration,  
15 corresponding to sensor quantities of 8, 27, and 64, respectively. The resulting prediction  
16 errors are denoted by red squares in Figure 5c. Additionally, we gradually increased the  
17 number of sensors from a small cube array to a large cube array, in the order of length,  
18 width, and height, thereby obtaining results for various irregular configurations with  
19 different quantities. The prediction errors for these configurations are represented by  
20 blue circles in Figure 5c. Despite the lack of a uniform configuration in the latter sensor  
21 arrays, they do not rigorously reflect the error levels across all configurations under  
22 the same quantity. However, they serve to bridge the gaps between adjacent cubic  
23 configurations, providing a more detailed characterization of the trend in prediction  
24 error with varying sensor quantities. Evidently, a higher quantity of sensors affords a  
25 more comprehensive information pool, thereby favoring the predictive capabilities of  
26 the prediction network[15]. However, this advantage is accompanied by a significant  
27 escalation in the cost and intricacy of array design[2]. Consequently, a delicate balance  
28 must be struck between the number of sensors and the precision of predictions. Fig.  
29 5c delineates PredNet validation error as the function of the number of sensors. For  
30 sensor quantities less than 8, a marked reduction in error is observed with an increasing  
31 number of sensors. Subsequently, this effect tends toward saturation, with negligible  
32 alterations post the deployment of 24 sensors. It is noteworthy that this decline is  
33 non-monotonic, suggesting the potential for an increase in error with a higher sensor  
34 count, a phenomenon also documented in previous study as a plausible manifestation  
35 of interference among distinct sensor inputs [10].  
36  
37  
38  
39  
40  
41  
42  
43  
44  
45

### 46 *3.4. Impact of sampling time*

47 Clearly, longer time series tend to contain richer information, but this comes with an  
48 increased sampling difficulty. Acquiring extensive samples over prolonged duration is  
49 often impractical in real-world applications. Here, we assess the impact of varying time  
50 series lengths on the network's predicting accuracy. The results in Fig. 5d indicate  
51 a gradual reduction in PredNet error with an increase in the duration of individual  
52 sequences. This effect approaches saturation after a sequence of 0.5s (corresponding to  
53 0.5 periods of undulation), with marginal improvement in positioning accuracy observed  
54 with further increases in duration.  
55  
56  
57  
58  
59  
60

Author guidelines for IOP Publishing journals in  $\text{\LaTeX}$  2 $\epsilon$

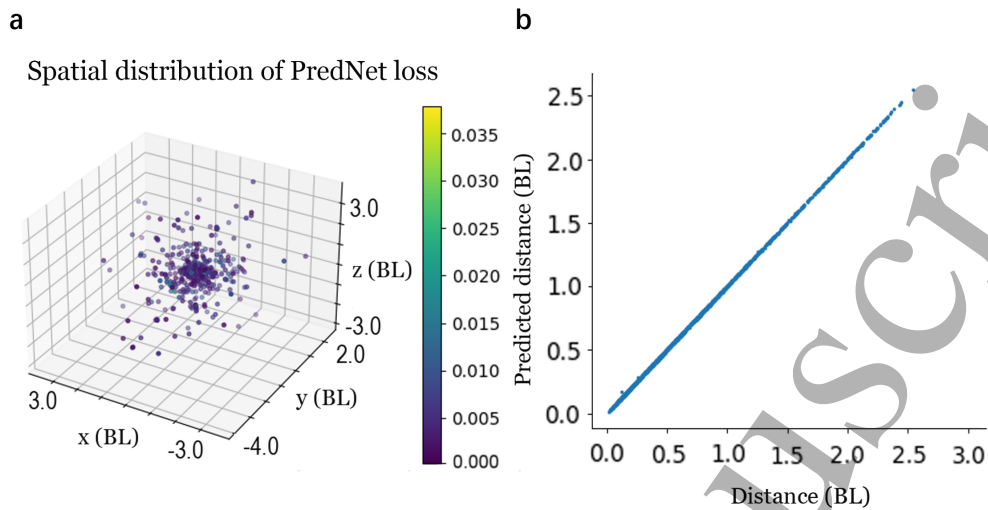


**Figure 4. (a) PredNet loss at different spatial positions. (b) PredNet predicted distance versus actual distance.** The distribution of PredNet errors on the validation set across spatial positions is presented. The results indicate that the PredNet demonstrates excellent predictive performance throughout the entire experimental range.

### 3.5. Impact of Signal-to-Noise Ratio

In practical applications, data sampled by sensors inevitably encompass the influence of various types of noise[15], such as complex water flow conditions, the inherent oscillation of the fish's body, or fluctuations in electronic device signals [15, 22, 27, 33]. To validate the robustness of PredNet and assess the impact of noise on localization performance, we compared the localization errors under different Signal-to-Noise Ratios (SNR). As depicted in Fig. 6a, with the continuous reduction in SNR, the accuracy of localization progressively declines, aligning with our expectations. Notably, this decline is non-linear, exhibiting a sharp increase in errors after SNR reaching 2.5, affirming that a certain level of noise does not compromise the identification of relevant information in the flow field by ALL. Additionally, the predicted distance as a function of actual distance under different SNRs is presented in Fig. 6b. It can be visually observed that the increasing noise predominantly affects areas farther from the fish, while proximal regions remain largely unaffected. This phenomenon arises due to the attenuation of the wake, resulting in smaller signal amplitudes in distant areas that are more susceptible to noise interference, aligning with physical principles.

### 3.6. Robustness of the prediction

We trained another neural network, ConfNet, to predict the reliability of the prediction results (see Method section for details). The outcomes, illustrated in Fig. 7a, reveal a stabilization of loss around 0.001 after approximately 50 epochs. Here, we present the distribution of ConfNet prediction errors relative to actual errors within

Author guidelines for IOP Publishing journals in  $\text{\LaTeX}$  2 $\epsilon$

10

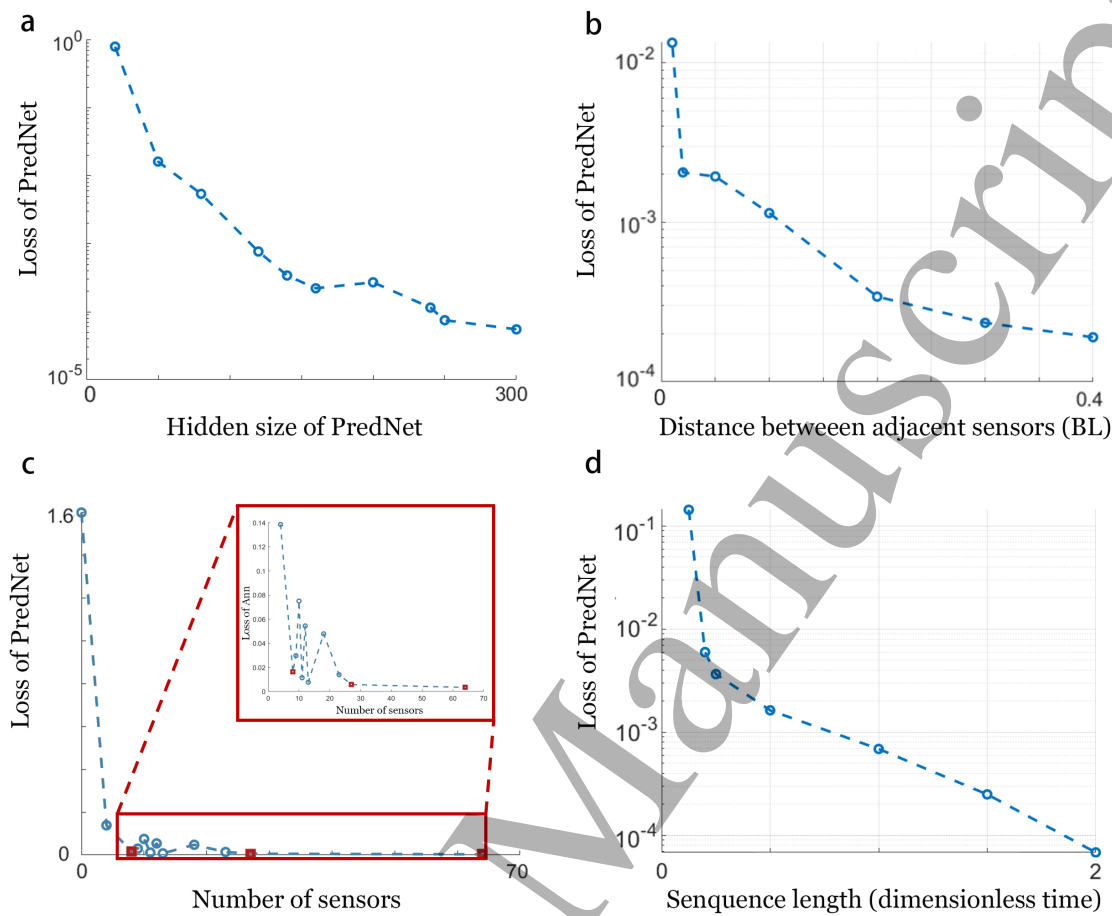


**Figure 5.** (a) PredNet loss on the validation set as the function of hidden size. (b) PredNet loss on the validation set as the function of adjacent sensors' distance. (c) PredNet loss on the validation set as the function of sensor quantity. The red squares represent the results obtained from a sensor array arranged in a standard cubic configuration, while the remaining data represents results obtained from randomly selecting the corresponding number of sensors from the cubic array. (d) PredNet loss on the validation set as the function of time sequence length.

the validation set (Fig. 7b). The perceptible alignment of the data distribution with a straight line suggests that ConfNet adeptly forecasts errors for data points at various positions. However, the accuracy of predictions decreases as the actual error increases. This can be attributed to the fact that data points with larger errors are fewer in number, and such points are often located farther from the fish's body. This implies that the vortex has already undergone sufficient decay, resulting in relatively less information, making it more challenging for the neural network to capture its features. Fig. 7d illustrates the distribution of ConfNet errors at different spatial positions, further demonstrating that the increased difficulty in prediction is due to the increasing distance.

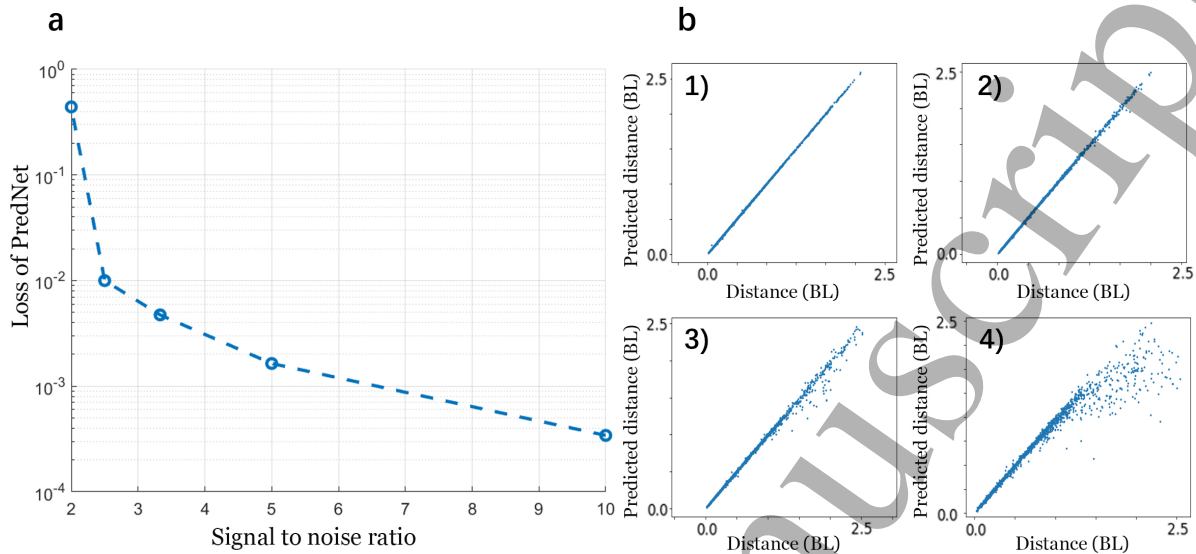


**Figure 6.** (a) PredNet loss on the validation set as the function of SNR. In this context, SNR is expressed as  $\text{SNR} = \frac{A_{sig}}{A_{noi}}$ , where  $A_{sig}$  denotes the average amplitude of the pressure signals and  $A_{noi}$  denotes the average amplitude of the noise. (b-e) Predicted distance versus actual distance for different SNR. Figure b to e represent scenarios with SNR of 10, 5, 3.3 and 2, respectively.

#### 4. Discussion

Our results numerically establish the practicality of employing the lateral line system to discern the position and pose of a free-swimming undulatory swimmer, which holds crucial implications for understanding the sensory mechanisms of fish. Previous studies have shown that fish predominantly rely on their lateral line for perception within a range of 5 body lengths (BL)[28]. So far, this perception method has been demonstrated at scales ranging from a few centimeters to several tens of centimeters, depending on the size of sensors[29]. In general, near-field hydrodynamic imaging functions effectively only over short distances, and is most accurate within this range. Our research demonstrates that accurate prediction of the position and posture of preceding fish can be achieved solely through pressure within a 4 BL range. This strongly suggests that vortex tails contain rich information about swimmers, which is valuable for understanding the functionality of biological lateral lines and designing artificial sensing systems. Our findings further affirm that the vortices generated by undulatory swimming, especially the pressure component, carry sufficient information about the swimmer, which enables information recipients to accurately identify its location and orientation within a 4BL distance.

In natural environments, sensors interact significantly with fluids. For instance, in the case of fish lateral line systems, the swimming motion of fish generates distinct flow patterns in their vicinity. This alteration of the ambient flow not only complicates

Author guidelines for IOP Publishing journals in  $\text{\LaTeX}$  2 $\epsilon$

12

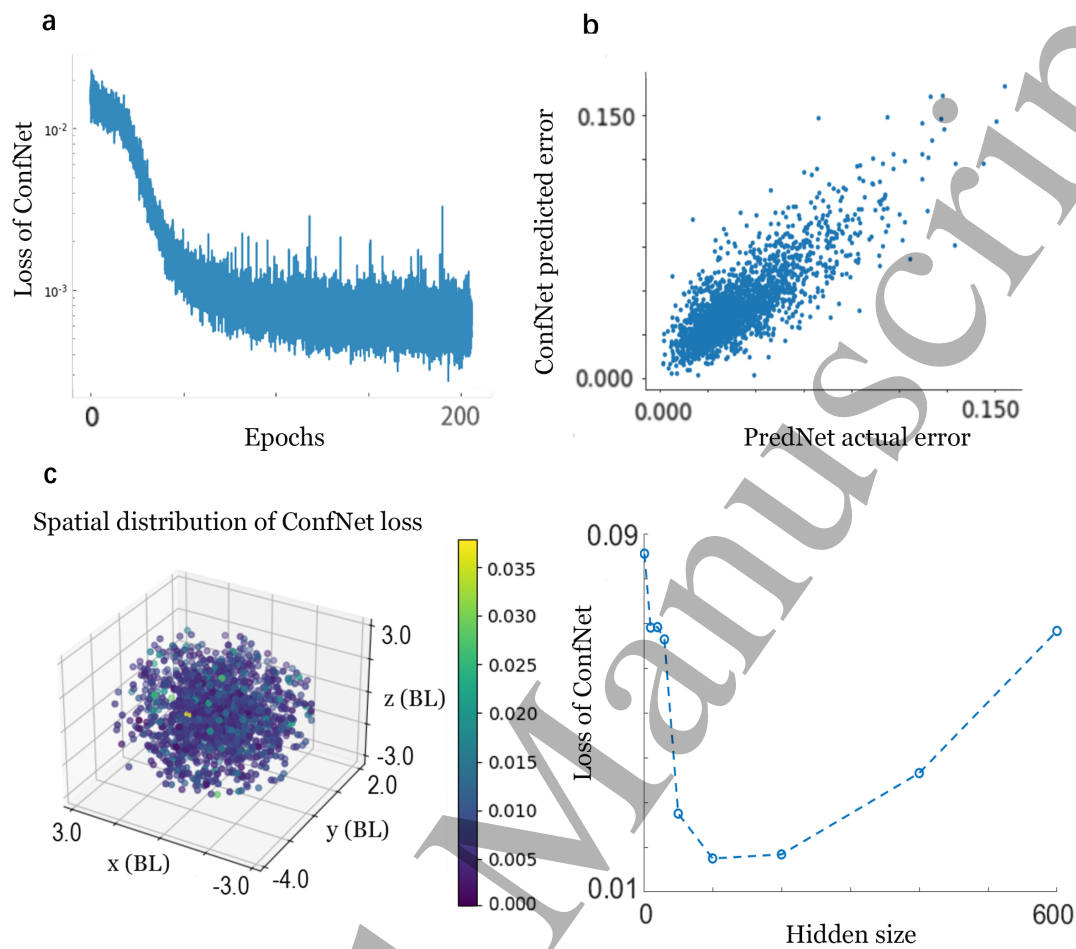


**Figure 7.** (a) Training loss for ConfNet as the function of training epoch. (b) Predicted error versus actual distance on the validation set. (c) Spatial distribution of ConfNet loss. (d) ConfNet loss as the function of hidden size. As the hidden size increases, the loss initially shows a decreasing trend, but starts to rise after the hidden size exceeds 200.

the existing flow dynamics but also poses challenges in acquiring accurate flow field information through the lateral line system. Therefore, the primary challenges in perceiving swimming fish in real-world scenarios encompass two aspects: extracting position and orientation-related features from the wake of the preceding fish, and mitigating the influence of sensor devices on the flow field. In this study, we primarily address the former issue by investigating the feasibility of identifying the position and orientation of a freely swimming mackerel based on pressure signals from an ideal sensor array. Although there remains a disparity compared to real perceptual scenarios, our findings hold significant implications. Moreover, disregarding the volume of the sensors endows our study with several irreplaceable advantages compared to many other studies. For instance, through coordinate transformation-based methods, we can obtain a wealth of training data encompassing various orientations of fish bodies. Otherwise, with a fixed sensor array in place, the computational costs required for CFD work would increase by

several thousand times, making training neural networks an almost unattainable task.

Evidently, both pressure and flow velocity, or shear information, hold significant importance. Perception in actual fish lateral line systems relies on both pressure and flow velocity signals simultaneously. Ideally, knowledge of one component allows for inference of the other, and the combined use of both signals can enhance prediction accuracy. However, simultaneously deploying two types of sensors significantly increases the complexity of design and sampling in practical applications. Here, we choose to utilize only pressure as the input signal, as artificial lateral line pressure sensors are more mature compared to velocity sensors and most ALL studies relied on pressure sensors. Thus, predictions based on pressure hold greater practical significance. Our findings confirm that pressure alone contains sufficient information of the position and orientation of swimmer. The consideration of shear information and their combined application will be the focus of our forthcoming efforts, tailored for more intricate environments and challenging perception tasks.

Our research holds significant implications for the mutual perception and schooling of multiple robotic fish. While ALL have demonstrated their utility in aiding underwater robots with increasingly complex perception tasks, the current ALL's sensing capabilities still lag far behind the lateral line of real fish. To the best of our knowledge, there is currently no mutual localization system for freely swimming robotic fishes. Our numerical results demonstrate the feasibility of achieving mutual localization in different directions based on vortex street interactions, providing insights into the design and arrangement of ALL. Looking ahead, we aim to factor in the influence of ALL on the flow field and apply our perception methods to real-world sensing challenges.

- [1] Ahmad T Abdulsadda and Xiaobo Tan. Underwater tracking of a moving dipole source using an artificial lateral line: algorithm and experimental validation with ionic polymer–metal composite flow sensors. *Smart Materials and Structures*, 22(4):045010, 2013.
- [2] Bingni W Brunton, Steven L Brunton, Joshua L Proctor, and J Nathan Kutz. Sparse sensor placement optimization for classification. *SIAM Journal on Applied Mathematics*, 76(5):2099–2122, 2016.
- [3] Brendan Colvert, Mohamad Alsalman, and Eva Kanso. Classifying vortex wakes using neural networks. *Bioinspiration & biomimetics*, 13(2):025003, 2018.
- [4] Sheryl Coombs and Sietse Van Netten. The hydrodynamics and structural mechanics of the lateral line system. *Fish physiology*, 23:103–139, 2005.
- [5] Branislava Curcic-Blake and Sietse M van Netten. Source location encoding in the fish lateral line canal. *Journal of Experimental Biology*, 209(8):1548–1559, 2006.
- [6] Branislava Curcic-Blake and Sietse M van Netten. Source location encoding in the fish lateral line canal. *Journal of Experimental Biology*, 209(8):1548–1559, 2006.
- [7] Ahmad Dagamseh, Remco Wiegerink, Theo Lammerink, and Gijs Krijnen. Artificial lateral-line system for imaging dipole sources using beamforming techniques. *Procedia engineering*, 25:779–782, 2011.
- [8] Guido Dehnhardt, Bjorn Mauck, Wolf Hanke, and Horst Bleckmann. Hydrodynamic trail-following in harbor seals (*phoca vitulina*). *Science*, 293(5527):102–104, 2001.
- [9] Jan-Moritz P Franosch, Andreas B Sichert, Maria D Suttner, and J Leo van Hemmen. Estimating position and velocity of a submerged moving object by the clawed frog *xenopus* and by fish—a cybernetic approach. *Biological cybernetics*, 93:231–238, 2005.
- [10] Florian Franzen. Object localization and classification by a simplified lateral line system of fish combined with neural networks.
- [11] Heidi L Fuchs, Gregory P Gerbi, Elias J Hunter, Adam J Christman, and F Javier Diez. Hydrodynamic sensing and behavior by oyster larvae in turbulence and waves. *The Journal of Experimental Biology*, 218(9):1419–1432, 2015.
- [12] F Hess and JJ Videler. Fast continuous swimming of saithe (*pollachius virens*): a dynamic analysis of bending moments and muscle power. *Journal of Experimental Biology*, 109(1):229–251, 1984.
- [13] AGP Kottapalli, Mohsen Asadnia, JM Miao, and MS Triantafyllou. Biomechanical canal sensors inspired by canal neuromasts for ultrasensitive flow sensing. In *2015 28th IEEE International Conference on Micro Electro Mechanical Systems (MEMS)*, pages 500–503. IEEE, 2015.
- [14] Guijie Liu, Huanhuan Hao, Tingting Yang, Shuikuan Liu, Mengmeng Wang, Atilla Incecik, and Zhixiong Li. Flow field perception of a moving carrier based on an artificial lateral line system. *Sensors*, 20(5):1512, 2020.
- [15] Yu Liu, Qiao Hu, Qian Yang, Tongqiang Fu, and Sihui Li. The relative perception system of underwater bionic vehicles based on the artificial lateral line pressure sensor array. *Flow Measurement and Instrumentation*, 93:102404, 2023.
- [16] Yu Liu, Qiao Hu, Qian Yang, Yixin Li, and Tongqiang Fu. An underwater moving dipole tracking method of artificial lateral line based on intelligent optimization and recursive filter. *Measurement Science and Technology*, 33(7):075113, 2022.
- [17] Tingyu Ming, Bowen Jin, Jialei Song, Haoxiang Luo, Ruxu Du, and Yang Ding. 3d computational models explain muscle activation patterns and energetic functions of internal structures in fish swimming. *PLoS computational biology*, 15(9):e1006883, 2019.
- [18] John Montgomery, Sheryl Coombs, and Matthew Halstead. Biology of the mechanosensory lateral line in fishes. *Reviews in Fish Biology and Fisheries*, 5:399–416, 1995.
- [19] John C Montgomery, Cindy F Baker, and Alexander G Carton. The lateral line can mediate rheotaxis in fish. *Nature*, 389(6654):960–963, 1997.
- [20] Saunvit Pandya, Yingchen Yang, Douglas L Jones, Jonathan Engel, and Chang Liu. Multisensor processing algorithms for underwater dipole localization and tracking using mems artificial lateral-line sensors. *EURASIP Journal on Advances in Signal Processing*, 2006:1–8, 2006.

- [21] Changlin Qiu, Zhengxing Wu, Jian Wang, Min Tan, and Junzhi Yu. Locating dipole source using self-propelled robotic fish with artificial lateral line system. *IEEE Transactions on Automation Science and Engineering*, 2023.
- [22] Changlin Qiu, Zhengxing Wu, Jian Wang, Min Tan, and Junzhi Yu. Locating dipole source using self-propelled robotic fish with artificial lateral line system. *IEEE Transactions on Automation Science and Engineering*, 2023.
- [23] Jialei Song, Haoxiang Luo, and Tyson L Hedrick. Three-dimensional flow and lift characteristics of a hovering ruby-throated hummingbird. *Journal of The Royal Society Interface*, 11(98):20140541, 2014.
- [24] Ralf C Staudemeyer and Eric Rothstein Morris. Understanding lstm—a tutorial into long short-term memory recurrent neural networks. *arXiv preprint arXiv:1909.09586*, 2019.
- [25] Eric D Tytell and George V Lauder. The hydrodynamics of eel swimming: I. wake structure. *Journal of Experimental Biology*, 207(11):1825–1841, 2004.
- [26] Pascal Weber, Georgios Arampatzis, Guido Novati, Siddhartha Verma, Costas Papadimitriou, and Petros Koumoutsakos. Optimal flow sensing for schooling swimmers. *Biomimetics*, 5(1):10, 2020.
- [27] Shane P Windsor, Stuart E Norris, Stuart M Cameron, Gordon D Mallinson, and John C Montgomery. The flow fields involved in hydrodynamic imaging by blind mexican cave fish (*astyanax fasciatus*). part i: open water and heading towards a wall. *Journal of Experimental Biology*, 213(22):3819–3831, 2010.
- [28] Shane P Windsor, Stuart E Norris, Stuart M Cameron, Gordon D Mallinson, and John C Montgomery. The flow fields involved in hydrodynamic imaging by blind mexican cave fish (*astyanax fasciatus*). part ii: gliding parallel to a wall. *Journal of Experimental Biology*, 213(22):3832–3842, 2010.
- [29] Ben J Wolf, Primoz Pirih, Maarja Kruusmaa, and Sietse M Van Netten. Shape classification using hydrodynamic detection via a sparse large-scale 2d-sensitive artificial lateral line. *IEEE Access*, 8:11393–11404, 2020.
- [30] Ben J Wolf, Steven Warmelink, and Sietse M van Netten. Recurrent neural networks for hydrodynamic imaging using a 2d-sensitive artificial lateral line. *Bioinspiration & biomimetics*, 14(5):055001, 2019.
- [31] Yingchen Yang, Jack Chen, Jonathan Engel, Saunvit Pandya, Nannan Chen, Craig Tucker, Sheryl Coombs, Douglas L Jones, and Chang Liu. Distant touch hydrodynamic imaging with an artificial lateral line. *Proceedings of the National Academy of Sciences*, 103(50):18891–18895, 2006.
- [32] Wei-Kuo Yen and Jenhwa Guo. Phase controller for a robotic fish to follow an oscillating source. *Ocean Engineering*, 161:77–87, 2018.
- [33] Xiande Zheng, Yong Zhang, Mingjiang Ji, Ying Liu, Xin Lin, Jing Qiu, and Guanjun Liu. Underwater positioning based on an artificial lateral line and a generalized regression neural network. *Journal of Bionic Engineering*, 15:883–893, 2018.
- [34] Xingwen Zheng, Chen Wang, Ruifeng Fan, and Guangming Xie. Artificial lateral line based local sensing between two adjacent robotic fish. *Bioinspiration & biomimetics*, 13(1):016002, 2017.
- [35] Xingwen Zheng, Wei Wang, Minglei Xiong, and Guangming Xie. Online state estimation of a fin-actuated underwater robot using artificial lateral line system. *IEEE Transactions on robotics*, 36(2):472–487, 2020.